remote sensing

MDPI

Article

The Multiple Perspective Response of Vegetation to Drought on the Qinghai-Tibetan Plateau

Yuying Zhu [1,2], Huamin Zhang [3], Mingjun Ding [1,2,*], Lanhui Li [4] and Yili Zhang [5]

[1] School of Geography and Environment, Jiangxi Normal University, Nanchang 330022, China
[2] Key Laboratory of Poyang Lake Wetland and Watershed Research, Ministry of Education, Jiangxi Normal University, Nanchang 330022, China
[3] Center for Natural Resources Policy Survey and Evaluation of Jiangxi Province, Nanchang 330025, China
[4] School of Computer and Information Engineering, Xiamen University of Technology, Xiamen 361024, China
[5] State Key Laboratory of Resources and Environmental Information System, Institute of Geographic Sciences and Natural Resources Research, Chinese Academy of Sciences, Beijing 100101, China
* Correspondence: dingmj@jxnu.edu.cn

Abstract: The Qinghai-Tibetan Plateau (QTP) is a global center of cold and dry, where the most extensive fragile alpine vegetation exists. Quantitative analysis of drought event characteristics and vegetation response to drought on the QTP is indispensable for understanding the increasing drought events in a warming climate which exacerbate adverse influence on extremely alpine ecosystems. Here, using the standardized precipitation evapotranspiration index (SPEI) and the normalized difference vegetation index (NDVI) from 2000 to 2018, this study analyzed the characteristics of drought events, their temporal impacts, and the stability of vegetation response to drought on the QTP. Results showed that: the characteristics of drought events on the QTP have clear spatial heterogeneity. When compared to the east monsoon region, most of the western regions have higher frequency and lower intensity of drought events. Drought has significant temporal effects on vegetation in grassland areas of the QTP during the growing season, which reach their peak in July and August. The 0–1-month and 3-month time scales were the optimal lagged and accumulated time during the growing season, respectively. The stability of vegetation response to drought showed significant spatial heterogeneity and varied with eco-geographical regions and vegetation types. Generally, forest areas showed high resistance (74.09) and resilience (2.26), followed by crop and grassland areas.

Keywords: drought; response; resistance and resilience; vegetation; Qinghai-Tibetan Plateau

check for updates

Citation: Zhu, Y.; Zhang, H.; Ding, M.; Li, L.; Zhang, Y. The Multiple Perspective Response of Vegetation to Drought on the Qinghai-Tibetan Plateau. *Remote Sens.* **2023**, *15*, 902. https://doi.org/10.3390/rs15040902

Academic Editor: Gabriel Senay

Received: 4 January 2023
Revised: 30 January 2023
Accepted: 3 February 2023
Published: 6 February 2023

Copyright: © 2023 by the authors. Licensee MDPI, Basel, Switzerland. This article is an open access article distributed under the terms and conditions of the Creative Commons Attribution (CC BY) license (https://creativecommons.org/licenses/by/4.0/).

1. Introduction

The frequency and intensity of drought have increased significantly as the global climate has changed [1–3]. There are complex properties and extensive effects of drought, so identifying and monitoring drought characteristics and their effects on terrestrial ecosystems are crucial challenges [4]. Additionally, accelerated dryland expansion has multiple consequences, including a decrease in carbon sequestration, enhancement of regional warming and land degradation, and desertification [5]. Therefore, many have studied drought events, their impacts on terrestrial ecosystems, and the responses and feedbacks of terrestrial ecosystems to drought [6,7].

Vegetation responds to drought from multiple perspectives, such as time-lag and cumulative effects [8]. The time-lag effects indicate that vegetation activity is significantly affected by the drought condition of the previous months [9], while the cumulative effects represent that the vegetation growth is affected by the cumulative drought condition over the previous months as well as the current month [4]. Previous studies showed that the time-lag effects of drought on vegetation growth were significant and different in varying vegetation types and regions [10–12]. However, these studies of drought just focused on

a single aspect, such as precipitation or temperature, and failed to fully capture the correlation between vegetation activity and integrated drought [10,12,13]. The standardized precipitation evapotranspiration index (SPEI) is an integrated drought index which can quantify the accumulated change in water availability [14]. SPEI can be used as an evaluation index to analyze the effects of drought on vegetation [4,11,15] and the cumulative effects of drought on vegetation can vary with vegetation types and growth stages [16–18]. However, a focus on both on the time-lag and cumulative effects of drought on vegetation growth has only been occasionally considered [19].

The stability (including resistance and resilience) of vegetation to drought interference is also widely considered in studies of global environmental changes [20–22]. Both resistance and resilience consider concurrent and delayed effects on ecosystems [23]. Experiments and modeling have analyzed these two stability indicators from species to biome levels [24–28]. However, these field experiments are limited by local natural conditions, human interference, and experimental cost. Moreover, conducting large-scale and long-term series research is impossible using field experiments [20]. Simulation quantification of tree ring data can solve some experimental defects [25,29,30], but non-tree vegetation types cannot be easily studied. Thankfully, satellite observations can obtain information across a wide range of space and time. Therefore, satellite observations, such as the fraction of absorbed photosynthetically active radiation (FAPAR) [31], space-borne solar-induced chlorophyll fluorescence (SIF) [26], and indicators of biomass and greenness of vegetation, such as the normalized difference vegetation index (NDVI) [20,32] and the enhanced vegetation index (EVI) [33,34], are applied in assessing the stability of vegetation.

The Qinghai-Tibetan Plateau (QTP) has a typical alpine climate and complex terrain and is a major sensitive area of global climate change [35,36]. Recent studies show that rapid warming over the QTP has partly improved the productivity of vegetation by influencing metabolism and prolonging the growth period [37–39]. Alpine grassland, the main vegetation type covering about two-thirds of the plateau, is deeply affected by climate change [40]. Specifically, the wetter grassland areas help vegetation grow [39,41–43], but enhanced drought in the southern and western parts of the QTP has degraded the local vegetation [42,43]. Most present efforts have focused on the impact of drought on vegetation at the basin or provincial scale for the same period on the QTP, ignoring the fact that drought influences current and future vegetation dynamics [44]. By contrast, the time-lag and cumulative effects of drought on vegetation and the stability of vegetation facing drought interference, especially for different vegetation types on the QTP, are rarely considered.

Therefore, our objective here is to understand the characteristics of drought events and how the various vegetation types responded to drought on the QTP. We used NDVI and SPEI data from 2000 to 2018, and analyzed the drought events and evaluated the time-lag and cumulative effects of drought on vegetation over the QTP during the growing season. The stability, i.e., resistance and resilience, of vegetation in response to drought was then quantified and compared.

2. Materials and Methods

2.1. Study Area

The QTP is located in southwestern China (67°40′37″–104°40′43″E, 25°59′26″–40°1′6″N) (Figure 1). It occupies about 1/4 of China's land area with an average elevation of 4320 m [45]. The average annual temperature ranges from −3.1 to 4.4 °C, the average annual precipitation ranges from 103 to 694 mm, and the QTP has an alpine climate [46,47]. The southeast is relatively warm and humid, while the northwest is cold and dry, with significant spatial differentiation. These unique natural conditions lead to extremely vulnerable vegetation ecosystems. Sub-tropical evergreen broad-leaved forest, deciduous broad-leaved forest, alpine shrub, alpine meadow, alpine steppe, alpine desert, and other vegetation types are mainly distributed from southeast to northwest of the QTP. The following are the eco-geographical regions of the QTP based on the actual variations of surface natural properties: IB1 means Golog-Nagqu high–cold shrub–meadow zone; IC1 means

Southern Qinghai high–cold meadow steppe zone; IC2 means Qiangtang high–cold steppe zone; ID1 means Kunlun high–cold desert zone; IIAB1 means Western Sichuan–eastern Xizang montane coniferous forest zone; IIC1 means Southern Xizang montane shrub–steppe zone; IIC2 means Eastern Qinghai-Qilian montane steppe zone; IID1 means: Ngari montane desert–steppe and desert zone; IID2 means Qaidam montane desert zone; IID3 means Northern slopes of Kunlun montane desert zone; OA1 means Southern slopes of Himalaya montane evergreen broad-leaved forest zone.

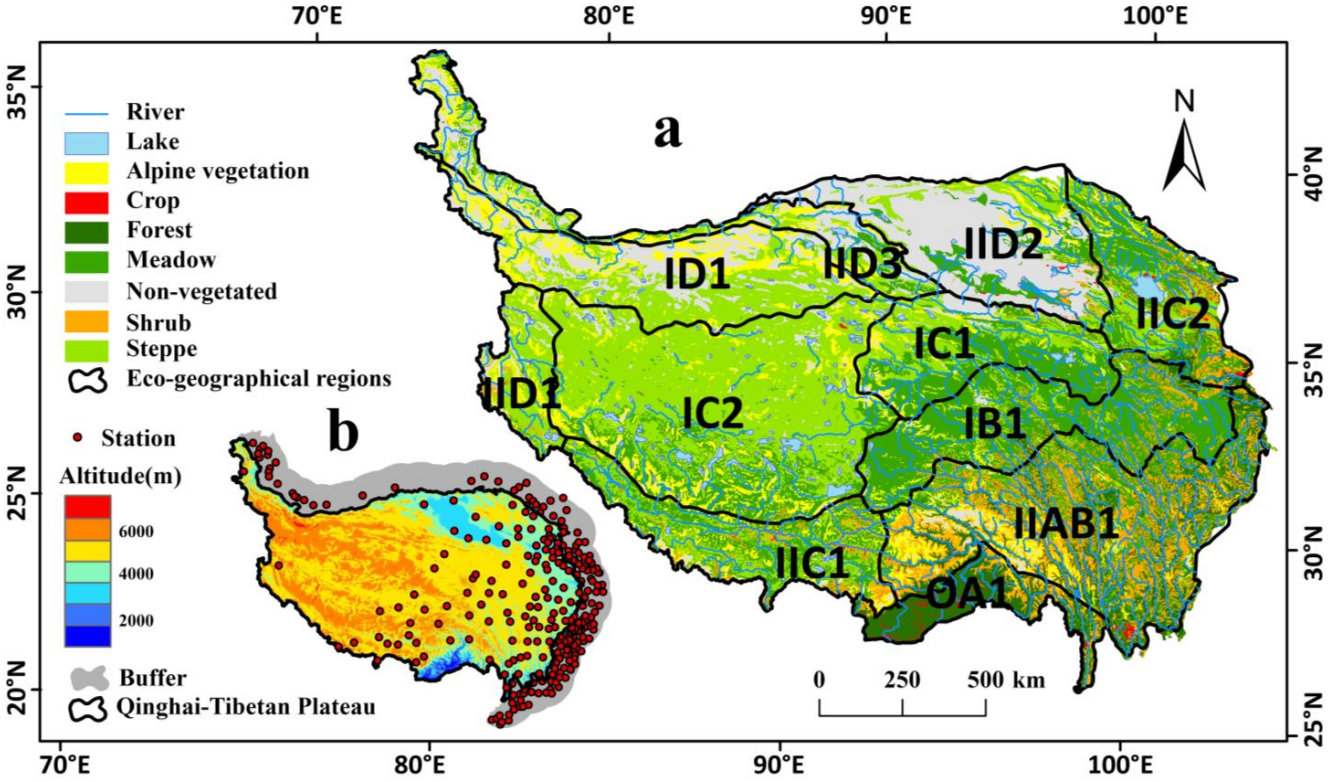


Figure 1. Spatial distribution of vegetation types (**a**) and meteorological stations (**b**) on the Qinghai-Tibetan Plateau (QTP).

2.2. Data and Preprocessing

We used 6 versions of MOD13A2 (Collection 6) NDVI data products from 2000 to 2018, and the datasets were collected from the National Aeronautics and Space Administration (NASA) (https://www.nasa.gov/, accessed on 28 November 2020). The spatial resolution is 1 km, and its temporal resolution is 16-day intervals. Moreover, the NDVI dataset was developed using the maximum value composition method (MVC) and minimized geometrical, atmospheric, and cloud effects. Then, the Savitzky–Golay method was used to smooth and reconstruct the NDVI data [48]. We defined the growing season as the period from May to September which is used to analyze vegetation response to drought in the growing season [35,37].

Meteorological data were collected from the National Meteorological Information Center (NMIC) of the China Meteorological Administration (http://www.cma.gov.cn/, accessed on 17 August 2021). We extended the study area 200 km outward (only for China) and added data of meteorological stations in the 200 km buffer zone to improve the accuracy of spatial interpolation. The potential evapotranspiration data were downloaded from the National Earth System Science Data Center, National Science & Technology Infrastructure of China (http://www.geodata.cn, accessed on 5 August 2022) [49].

Vector boundary data of the QTP were obtained from the Institute of Geographic Sciences and Natural Resources Research, Chinese Academy of Sciences. The vector data of QTP ecogeographical regionalization were derived from the Ecological Geographical

Regions Map of China (http://www.resdc.cn/, accessed on 28 November 2020), which is primarily based on the actual variations of surface natural properties. Combinations of temperature and humidity conditions and zonal vegetation and soil types can lead to a better understand the basic natural conditions of the surface of the plateau [50]. The land cover map of the QTP was extracted from the 1:1,000,000 digitalized vegetation map of China (Editorial Board of Vegetation Map of China, 2001, https://www.resdc.cn, accessed on 28 November 2020).

2.3. Methods

2.3.1. Analysis of the Spatial Pattern of Drought Characteristics

SPEI normalizes the cumulative probability value of the difference between precipitation and potential evapotranspiration (D_i), the degree of deviation between D_i, and its average state reflects the drought characteristics in a certain area [14,51]. SPEI values with the time scales of 1, 2, 3, and 12 months from 1972 to 2018 were calculated using the revised model in 2014 to analyze the characteristics of drought events and vegetation response to drought on the QTP from 2000 to 2018 [52], following:

$$D_i = P_i - PET_i \quad (1)$$

where D_i is the difference between the precipitation P and PET for the month i (profit and loss, mm), P_i is the precipitation of the month i (mm), and PET_i is potential evapotranspiration of the month i (mm). The potential evapotranspiration was calculated using Penman–Monteith equations based on meteorological data such as precipitation, temperature, and relative humidity. Then, the monthly aggregated D at multiple time scales were normalized at length into three-parameter log-logistic probability distributions to obtain the SPEI. We used the SPEI package in R 4.1.3 to calculate SPEI (https://CRAN.R-project.org/package=SPEI, accessed on 17 August 2021). The SPEI data of original meteorological stations were interpolated to a raster surface with 1 km spatial resolution using ANUSPLIN software. Previous studies have shown that this method is effective in interpolating meteorological data [53,54].

A drought event is considered to occur when the SPEI-12 of a given month and at least two consecutive months thereafter is below a certain threshold [55]. The average of the twelve SPEI-12 monthly values per year is taken as the annual SPEI-12. The tenth percentile of annual SPEI-12 from 1972 to 2018 was used to obtain the drought threshold. We quantified drought intensity using mean values of SPEI-12 during drought events [34]. For each pixel, we calculated the frequency of drought events and the average value of drought duration and drought intensity to analyze the characteristics of drought events. When the SPEI value is less than -0.5, it indicates the occurrence of drought, which can be further classified as mild drought ($-1 < \text{SPEI} \leq -0.5$), moderate drought ($-1.5 < \text{SPEI} \leq -1$), severe drought ($-2 < \text{SPEI} \leq -1.5$), and extreme drought ($\text{SPEI} \leq -2$) [56]. In addition, precipitation divided by potential evapotranspiration was used to calculate the aridity index (AI) in order to evaluate the dryness of the QTP [41]. Specifically, hyper-arid ($\text{AI} < 0.05$), arid ($0.05 \leq \text{AI} < 0.2$), semi-arid ($0.2 \leq \text{AI} < 0.5$), sub-humid ($0.5 \leq \text{AI} < 0.75$), and humid ($\text{AI} > 0.75$) [41].

2.3.2. Temporal Effects of Vegetation Response to Drought

We calculated Pearson correlation coefficients (r) between NDVI and each time scale SPEI to explore the temporal effects of vegetation in response to drought on the QTP. As the temporal effects on the monthly scale are generally shorter than a quarter [9,57], the time scale of time-lag and cumulative effects was set to 0–3 months and 1–3 months, respectively. We calculated the correlation coefficients (r_0, r_1, r_2, r_3) of the NDVI and 1-month SPEI at each lagged time (i) to evaluate the vegetation time-lag response to drought:

$$r_i = corr(NDVI, SPEI_i) \quad 0 \leq i \leq 3 \quad (2)$$

$$r_{max-lag} = \max(r_i) \quad 0 \le i \le 3 \tag{3}$$

where r_i is the correlation coefficient between the monthly NDVI time series (2000–2018) and 1-month SPEI, i is the time-lag time from 0 to 3 (0 indicates no time-lag effects), $r_{max-lag}$ is the maximum value of r_i. The lag month i with the optimum correlation is taken as the optimum time-lag.

Pearson correlation coefficients between the monthly NDVI and multi-time scale SPEI were considered as potential indicators for cumulative responses of vegetation to drought:

$$r_j = corr(NDVI, SPEI_j) \quad 1 \le j \le 3 \tag{4}$$

$$r_{max-cum} = \max(r_j) \quad 1 \le j \le 3 \tag{5}$$

where r_j is the correlation coefficient between the month NDVI time series (2000–2018) and multi-time scale (j) SPEI, j is the accumulated time from 1 to 3, and $r_{max-cum}$ is the maximum value of r_j.

2.3.3. Evaluation of the Resistance and Resilience of Vegetation in Response to Drought

We used resistance and resilience to measure the stability of vegetation in response to drought. They were calculated on the interannual scale [33]. Resistance is expressed as the ability of an ecosystem to maintain its original levels of functioning during drought [31]. Resilience defines the capacity for ecosystem functioning to recover to the normal state after droughts [20,31]. For each pixel, drought years were judged according to the SPEI threshold. Since the drought years occurred more than once, we averaged the two stability indicators. We found that there are a small number of extremely high values of the resistance and resilience that affect the results. Thus, we removed the largest 5% of the two stability indicators in the subsequent analysis [34]. The equations for resistance (Ω) and resilience (Δ) are [28]:

$$\Omega = \frac{\overline{Y_n}}{\left|Y_e - \overline{Y_n}\right|} \tag{6}$$

$$\Delta = \left|\frac{Y_e - \overline{Y_n}}{Y_{e+1} - \overline{Y_n}}\right| \tag{7}$$

where Y_n, Y_e, and Y_{e+1} represent the expected NDVI during normal years (mean across all the non-extreme years), during the year climate extremes occurred and during the year after a climate extreme, respectively.

3. Results

3.1. Spatial Patterns of Drought Event Characteristics

The drought event characteristics of the QTP from 2000 to 2018 are shown in Figure 2. The drought frequency in most areas of the QTP ranged from 3 to 9, accounting for 75.04% of the total area (Figure 2a). Regions with drought frequency $\le$3 accounted for 22.6% of QTP, mainly distributed in the north–center of cold and arid regions. Areas with drought frequency $\ge$9 accounted for 2.36%, mainly distributed in the southwest of the QTP, especially in the Qiangtang Plateau and Ngari region. The mean drought duration was 3 to 7 months, accounting for 89.91% of the total QTP (Figure 2b). Regions with drought duration $\ge$7 months were mainly distributed in humid and semi-humid zones (part of IIAB1) and arid zones (IID2). Figure 2c shows that the mean drought intensity was -1.5 to -0.6 on the QTP, mild drought and moderate drought, with moderate drought accounting for 72.8% of the total plateau. Overall, the drought characteristics show significant spatial heterogeneity on the QTP. Compared with the eastern monsoon region, most of the western regions have higher frequency and lower intensity of drought events.

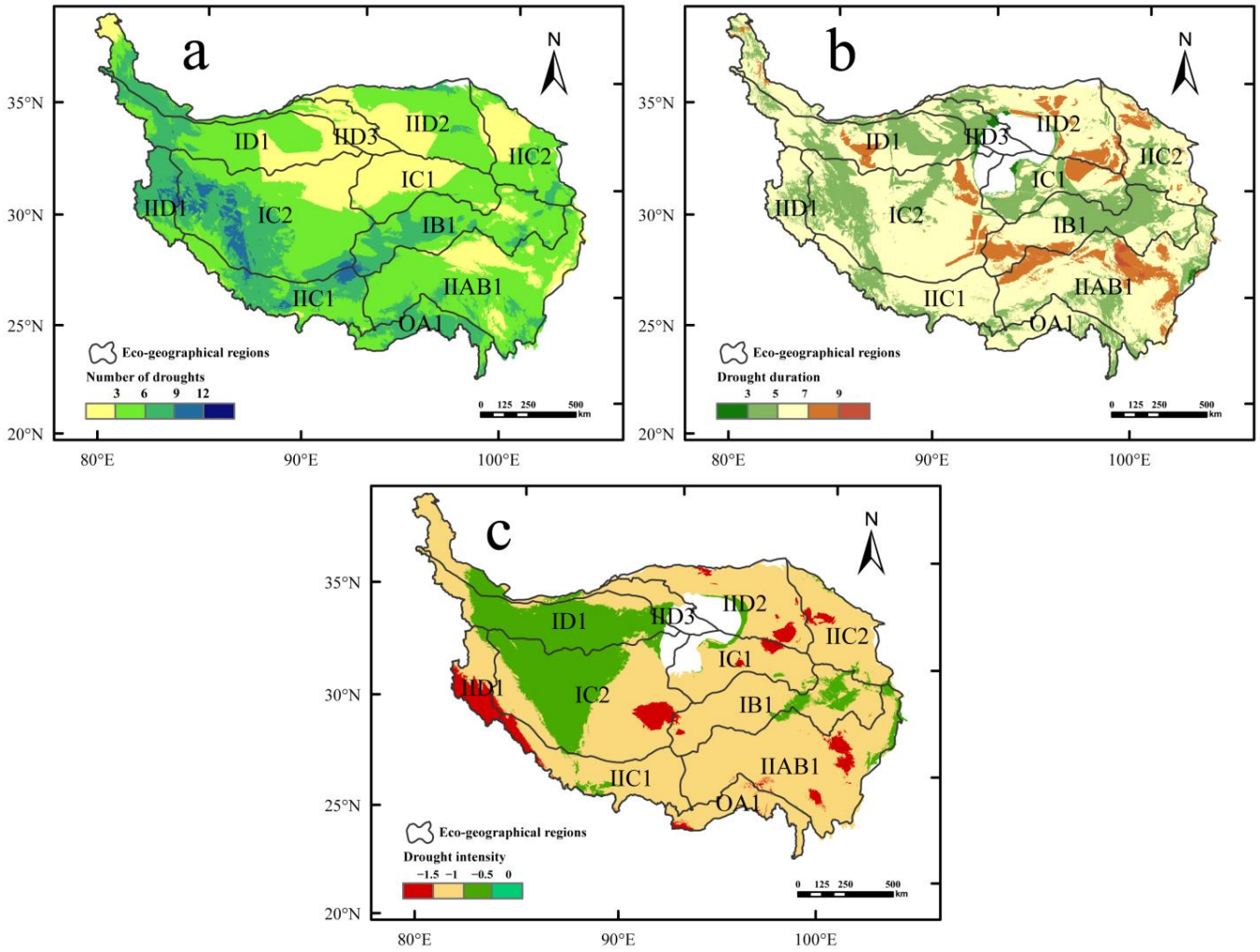


Figure 2. Spatial pattern of drought on the QTP from 2000 to 2018. (**a**) The number of droughts, (**b**) drought duration (month), and (**c**) drought intensity.

3.2. Spatial Patterns of the Time-Lag Effects of Drought on Vegetation during the Growing Season

Figure 3 shows the maximum correlation ($r_{max-lag}$) of 1-month SPEI with NDVI in the growing season. From May to September, the area with significant time-lag response showed an increasing trend. The significant response regions accounted for the largest proportion (33.1%) in July. The grassland area in the south of IC2, IIC1, IIC2, IC1, and the east of IB1 were dominated by significantly positive correlations.

In the view of lagged months, the 0-month lag had the largest area (43.7% and 33.39%) during May and July, including alpine grassland of IC2, IIC1, IC1, IB1, and IIC2 (Figure 4). The $r_{max-lag}$ at time-lags of one-month occupied most of the area (34.17%, 35.24%, and 43.7%) during other months (June, August, and September). These areas were mainly located in alpine grasslands (IC2, IC1, and IB1) and temperate mountain steppes (IIC1 and IIC2).

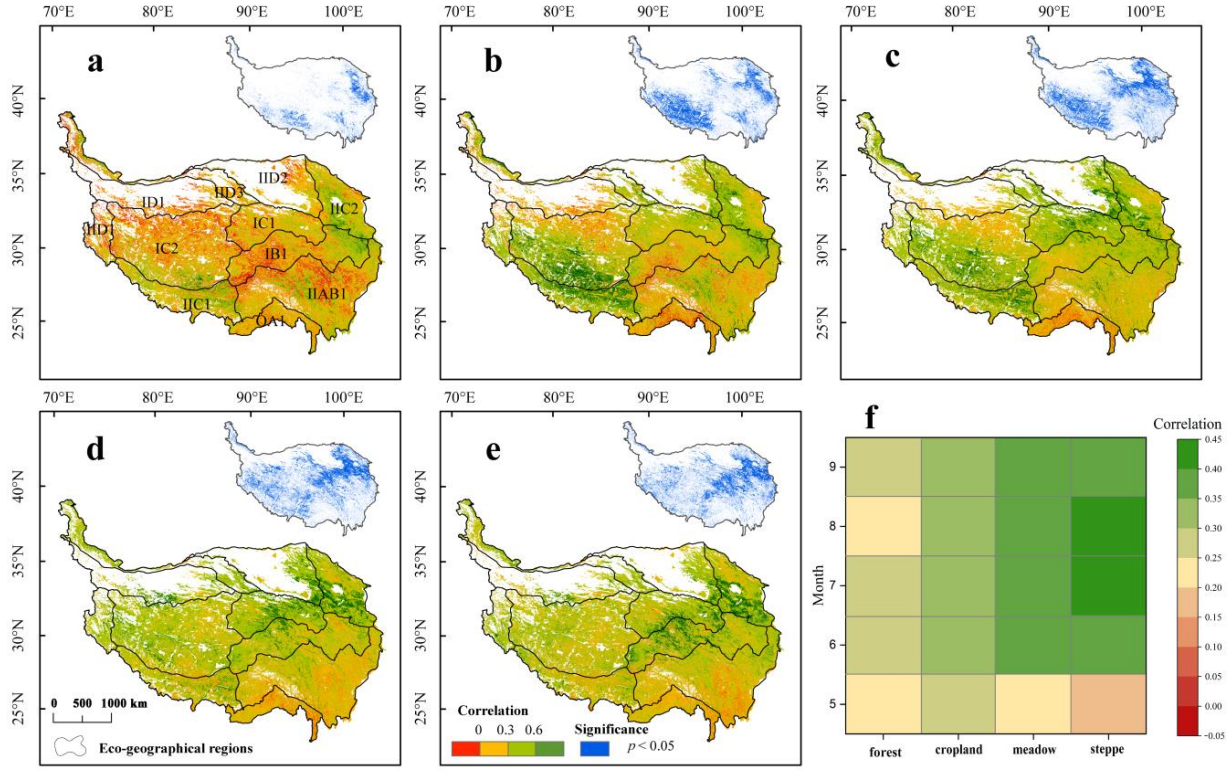


Figure 3. Spatial distribution of the largest correlation coefficient $r_{max-lag}$ between one-month SPEI and NDVI and significance ($p < 0.05$) from 2000−2018. (**a**) May; (**b**) June; (**c**) July; (**d**) August; (**e**) September. The largest correlation coefficient $r_{max-lag}$ between SPEI and NDVI of different vegetation types on the QTP (**f**).

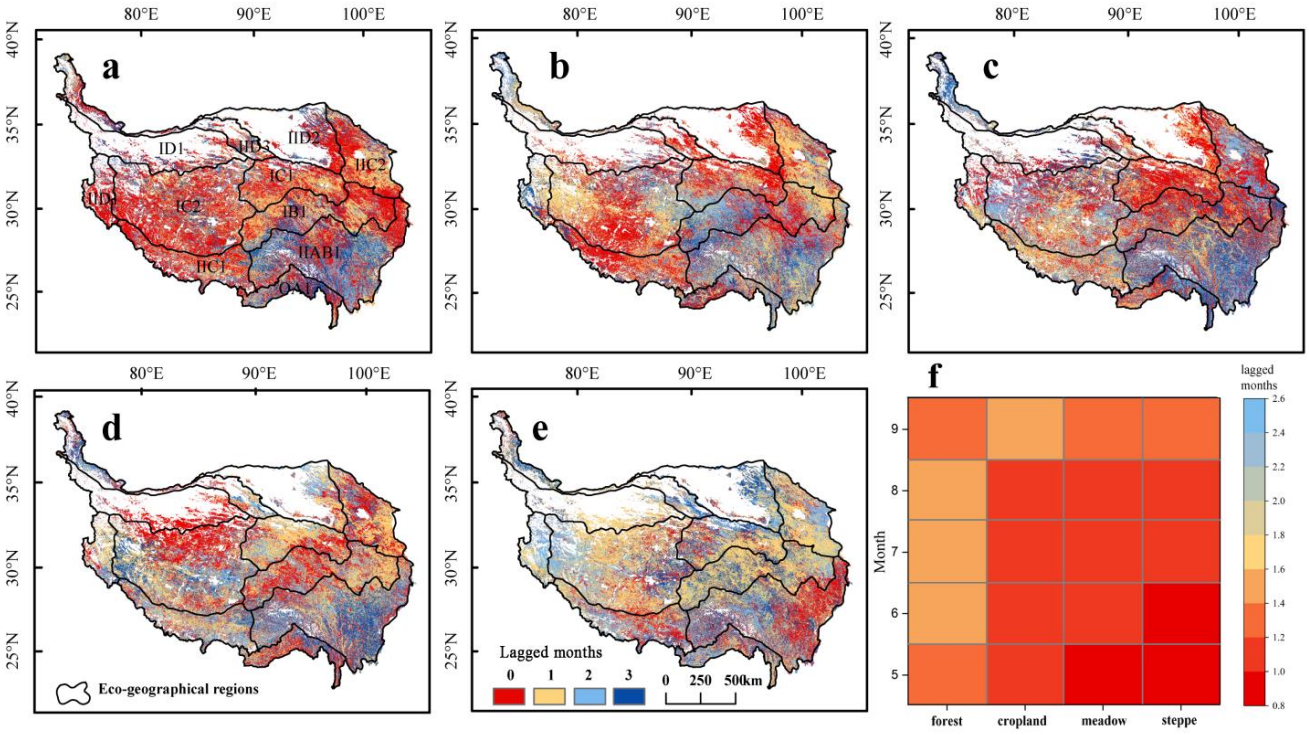


Figure 4. Spatial distribution of the corresponding lagged months where the largest correlation coefficient $r_{max-lag}$ occurred. (**a**) May, (**b**) June, (**c**) July, (**d**) August, and (**e**) September. The corresponding lagged months (i) of different vegetation types when $r_{max-lag}$ occurred (**f**).

Figures 3f and 4f show the difference in drought time-lag response of different vegetation types in the growing season, indicating that drought had increased time-lag effects on the steppe and meadow within shorter time scales when compared to other vegetation types. However, the time-lag response of forests was not clear and the corresponding lagged months were longer. In general, vegetation on the QTP has a time-lag response to drought, and the time-lag response effect was more obvious in steppe and meadow areas.

3.3. Spatial Patterns of the Cumulative Effects of Drought on Vegetation during the Growing Season

There is a significant positive correlation between NDVI and the multi-time scale SPEI from June to September for more than 25% of the total plateau, indicating sensitivity of vegetation to the drought (Figure 5). The spatial distribution of significant time-lag effect and cumulative effect showed high correspondence. However, the overall correlation coefficient of cumulative effects was lower than time-lag effects.

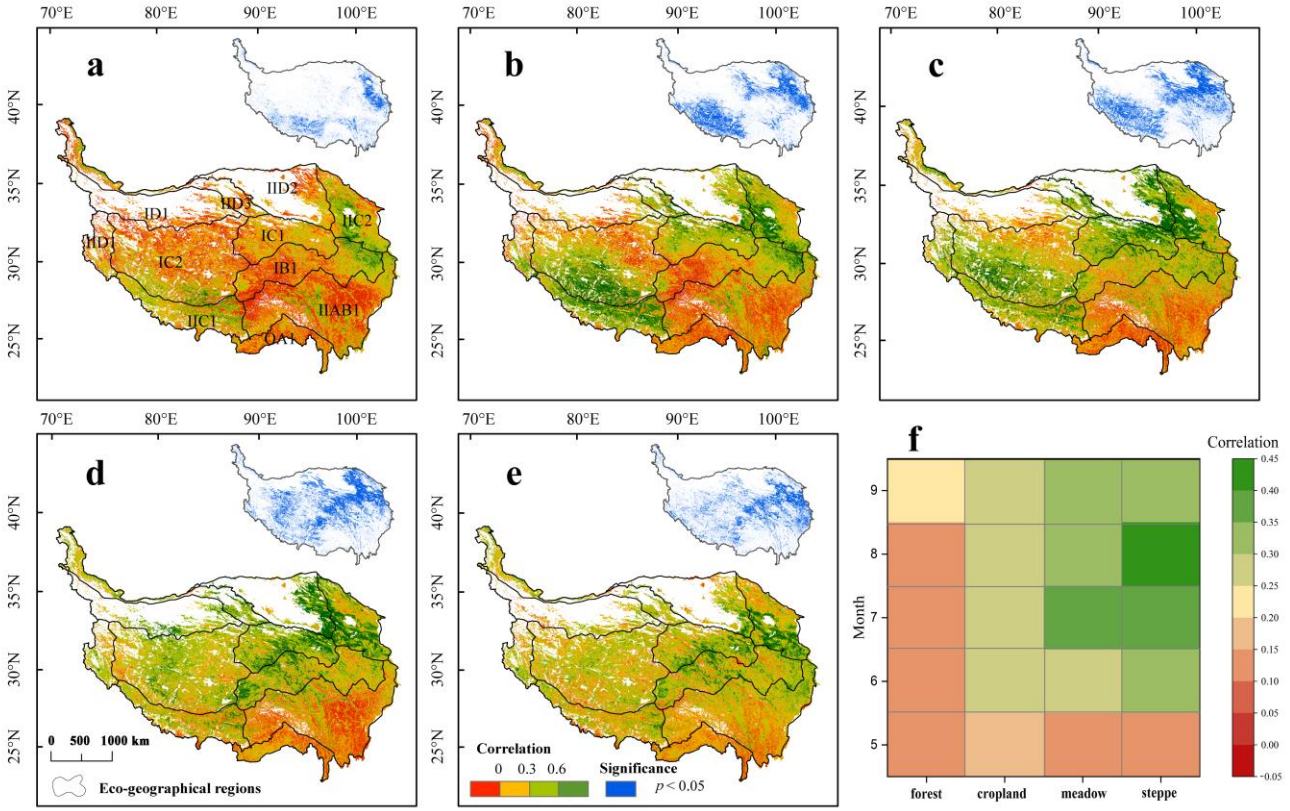


Figure 5. Spatial pattern of the largest correlation coefficient $r_{max-cum}$ between SPEI and NDVI and significance ($p < 0.05$) from 2000−2018. (**a**) May; (**b**) June; (**c**) July; (**d**) August; (**e**) September. The largest correlation coefficient $r_{max-cum}$ between SPEI and NDVI of different vegetation types on the QTP (**f**).

At different stages of the growing season, the cumulative effects showed significant spatial differences between different time scales (Figure 6). In May, 48.5% of the QTP presented one-month cumulative effect to drought. However, the $r_{max-cum}$ at a cumulative effect of three months gradually dominated from June to September. The response areas were distributed in the sub-polar and temperate semi-arid grassland of the QTP (IC2, IC1, IIC1, IIC2, and IIAB1), and the distribution of these areas expanded gradually.

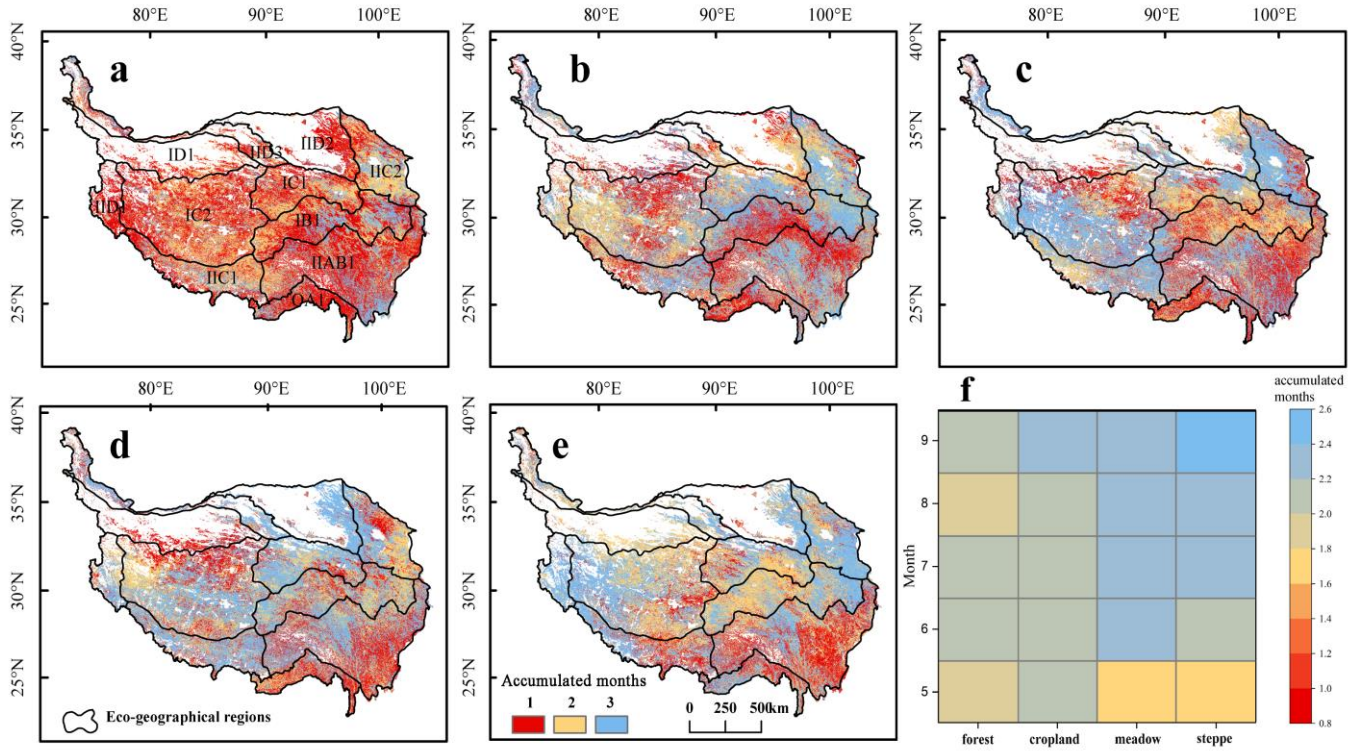


Figure 6. Spatial distribution of the corresponding accumulated months when the largest correlation coefficient $r_{max-cum}$ occurred. (**a**) May; (**b**) June; (**c**) July; (**d**) August; (**e**) September. The corresponding accumulated months (i) of different vegetation types when $r_{max-cum}$ occurred (**f**).

Figures 5f and 6f show that the cumulative response of forests to drought was relatively poor. By contrast, drought increased cumulative effects on the steppe and meadow within longer time scales when compared to other vegetation types in the growing season. On the whole, the spatial distribution of cumulative effects of vegetation on drought exhibited more significant differences when compared with the time-lag effect. Grassland was more sensitive than other vegetation types to the cumulative response of drought during the growing season.

3.4. Spatial Pattern of Resistance and Resilience to Drought

Figure 7 exhibits the regional differences of resistance and resilience to drought on the QTP over the past 20 years. Most values of resistance on the QTP were less than 75, accounting for 82.33% (Figure 7a). In addition, the distribution of areas with relatively high resistance (>75) was concentrated in major steppe and forest eco-geographical regions that are located in the junction of IC2, IC1, and IID3, the north of IC2, and most of OA1 and IIAB1. Figure 7b shows the resilience values of the south of IC2, IID1, IIC1, west of IB1, east of IC1, IID2, southwest of IIAB1, and east of OA1 were mainly between 1 and 3 (42.51%). Areas (39.23%) with resilience less than 1 were mainly concentrated in grassland areas in the northern and eastern parts of the QTP. Relatively high resilience was seen only in forest areas (OA1 and parts of southern IIAB1). Figure 7 shows the resistance and resilience of main vegetation types on the QTP. The forest has the highest resistance, followed by crop and steppe, while the meadow has the lowest resistance. For the resilience, the descending order is crop, forest, meadow, and steppe.

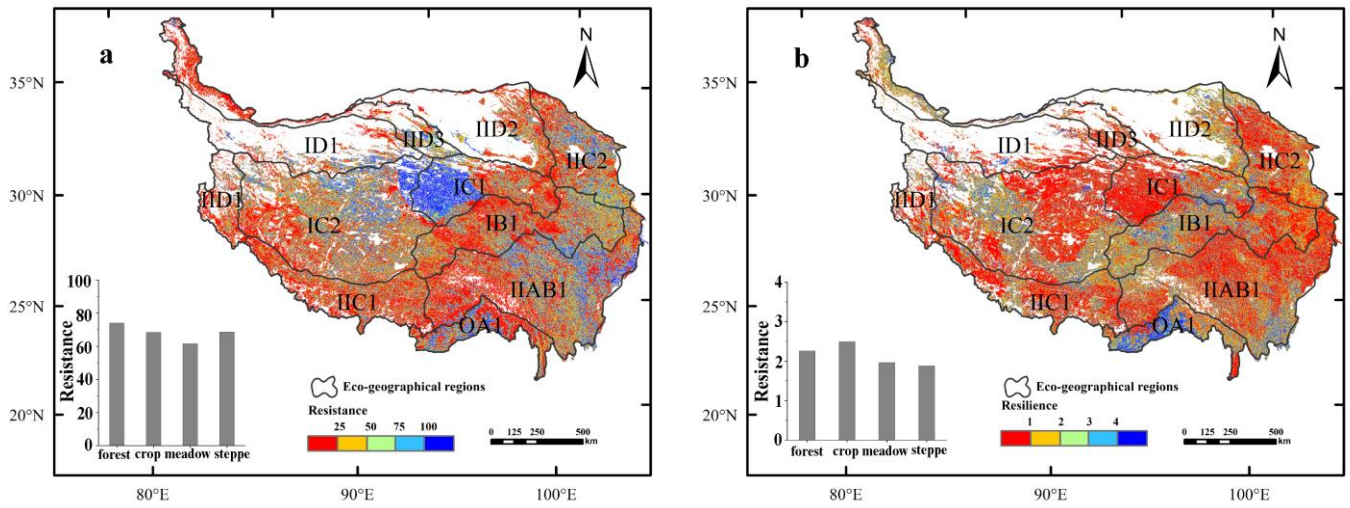


Figure 7. Spatial pattern of resistance (**a**) and resilience (**b**) of vegetation to drought and the differences in resistance and resilience between vegetation types on the QTP from 2000 to 2018.

4. Discussion

4.1. Divergent Temporal Response of Vegetation to Drought

The complexity and intrinsic multi-scalar characteristic of drought makes it difficult to understand the response of vegetation [4]. Fang et al. [58] pointed out that the highest vegetation vulnerability to drought stress is in the summer months. Here, we have considered the temporal effects of drought on vegetation growth season. Previous studies have proved that vegetation growth is more affected by early drought and does not respond significantly to changes in the present water condition [11,59]. Our study found that the forest response to drought is weak (Figures 3f and 5f). The reason may be that most of the woody vegetation areas of the QTP are located in the humid area and sub-humid area and local climate changes are relatively mild [60,61]. Woody vegetation can absorb more available soil water deeper by thick and deep roots [62], and the xylem water [63], rich storage of carbohydrates [8], and the strategies for coping with drought events [64] make woody vegetation more insensitive to drought than other vegetation types. However, most of the steppe on the QTP is located in arid and semi-arid areas [60] and plant roots are relatively shallow. Consequently, the temporal effects of the vegetation response are more sensitive. We also found that the drought sensitivity of the steppe in July and August was higher because of the "water sensitive period" of vegetation for water demand during this period, leading to vegetation sensitivity to water changes [65]. There was a consistency between the temporal effects of the meadow and steppe response to drought in the growing season. Our study provides further evidence that the temporal effects of vegetation response to drought are influenced by the environmental conditions at that time and vegetation species [9,11]. However, droughts monitored by SPEI on a monthly time step are not precise enough in detecting the onset, end, and cumulative stress of drought [66]. In addition, SPEI considers only the cumulative amounts of deficit/surplus water availability within a certain period of time, but does not consider the internal distribution of those variables [67], which undoubtedly has an important impact on vegetation growth. Therefore, the uncertainty caused by the limitations of SPEI needs further study.

4.2. Differences in Resilience and Resistance of Vegetation Types

The resistance and resilience of different vegetation types are clearly different due to their physiological structure, internal physiological mechanism, and strategies for coping with extreme climate events [4,68]. Additionally, differences in environmental conditions and species diversity lead to regional differences in the stability of the same vegetation type [29,34]. We found significant differences in resistance and resilience under different dry

and wet conditions (Figure 7), which confirmed the above statements. Figure 8 illustrates that the resistance of the areas with AI lower than 0.75 (arid, semi-arid, semi-humid regions) continued to rise, while the resistance of the areas with AI higher than 0.75 (humid region) showed a negative correlation with AI on some intervals. Vicente-Serrano et al. [4] obtained similar results that sub-arid and sub-humid communities can withstand water deficits. The relatively high resistance of semi-arid and sub-humid regions also makes the difference in coverage after vegetation drought restoration smaller, so the resilience was relatively low. The resilience of areas with AI higher than 1 was positively correlated with AI. It may be that the higher biodiversity of the humid region enables vegetation to recover and even exceed original productivity as soon as possible after experiencing severe drought [62,69]. In addition, the intervention of the human activity makes the resistance and resilience of the crop higher than natural conditions. This is because crops planted on farms are typically chosen to be more flexible and the breeding of the species, timely meteorological monitoring, and artificial water supplement (irrigation) also greatly increased the adaptation of plants to climate change.

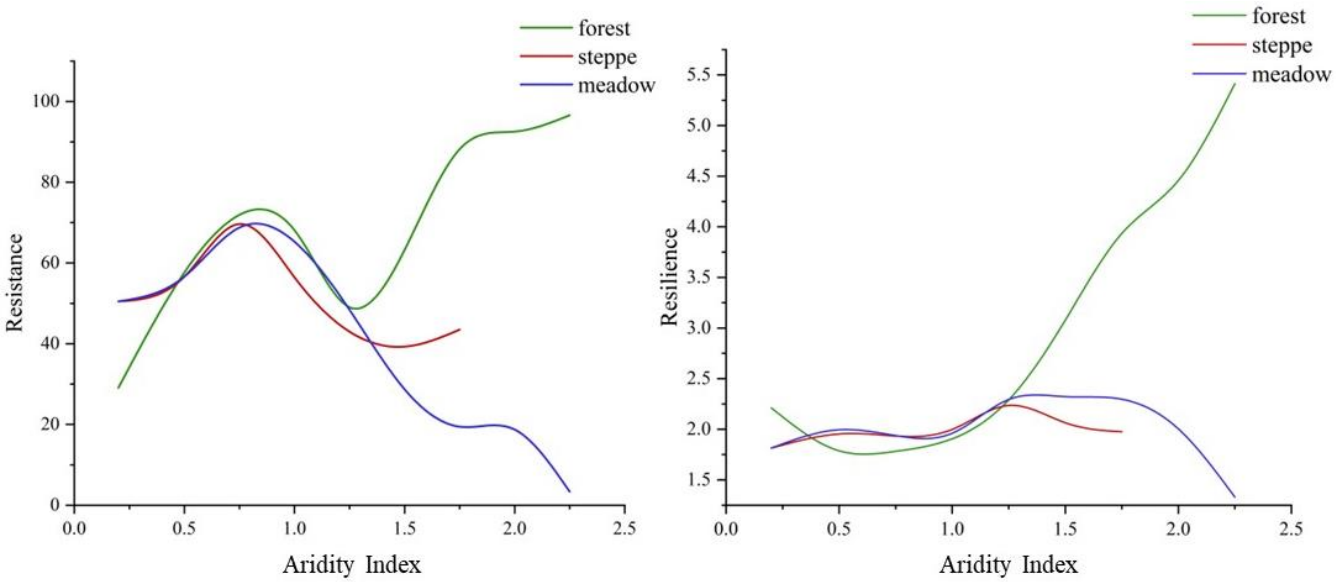


Figure 8. Variation of vegetation stability under different wet and dry conditions on the QTP.

4.3. Implication for the Ecological Protection of the QTP

The southeast of the QTP is influenced by the East Asian and South Asian monsoons with a lot of water vapor [70], where the water condition is superior and the annual precipitation is higher than the potential evapotranspiration [47,71]. However, the northwestern region is dominated by westerly and northerly winds with dry air and less precipitation [70]. This pattern of climate results in an increase in aridity from the southeast to the northwest [60]. The arid/semi-arid areas are characterized by limited vegetation growth due to water shortages [72,73] where precipitation is low and rising surface air temperature has accelerated evaporation [73,74]. Our study also shows that drought in arid and semi-arid areas of the QTP is characterized by high frequency and a close relationship between drought and vegetation in the growing season (Figures 2, 3 and 5). The water conditions in the southeastern QTP are wetter, and the annual precipitation is higher than the potential evapotranspiration [47,71]. However, the unusual activity of the monsoon also makes local climatic conditions relatively unstable, causing long periods of intense drought events. Other studies have also pointed out that drought has become more frequent and intense in the southwest, northwest, and parts of the southeast of the QTP at present or may do so in the future [75]. Therefore, these regions are the key areas to focus on the influence of drought on vegetation in the future.

We also found that the degree of response and the resistance of grassland to drought are high and strong. However, once affected by drought, the resilience of grassland can weaken later. We also found that the resilience of the grassland distributed in the arid and semi-arid areas of the QTP was weaker than that of the grassland in other areas, even though they were the same vegetation type, which may also be significantly related to the differences in local hydrothermal conditions. At present, China has carried out a large number of ecological protection projects in the grassland areas of the QTP [53,76]. Based on our results, we suggest that these projects should pay more attention to the grassland in the arid and semi-arid areas of the QTP. For example, in the same productive grassland, the grazing capacity of grassland in arid and semi-arid regions should be lower than in other regions. In addition, more protected areas could be established on grasslands for long-term management of this ecosystem type. In addition, according to different vegetation types during different stages of the growing season, drought should be monitored at appropriate time scales, and corresponding drought management measures can then be carried out in a timely manner.

5. Conclusions

It is necessary to assess the impacts of drought on the vegetation, especially on the QTP, which is extremely sensitive to climate change. Here, we found that the characteristics of drought events show significant spatial heterogeneity on the QTP. Compared with the eastern monsoon region, most of the western regions have higher frequency and lower intensity of drought events. A significant temporal effect of vegetation response to drought existed in grassland areas of the QTP. The maximum correlation coefficient and its corresponding time scale had clear spatial and temporal differences aligned with the growing season. The difference in environmental conditions and drought resistance of vegetation means that forest was relatively insensitive to drought. However, herbaceous plants (steppe and meadow) were more sensitive to drought, especially in July and August. There were significant differences in drought resistance and resilience among different vegetation types. Forest showed high resistance and resilience, following by crop and grassland. However, due to the limitations of SPEI, it is uncertain when analyzing the characteristics of vegetation response to drought.

Author Contributions: Y.Z. (Yuying Zhu): Methodology, data curation, and writing—original draft. H.Z.: Writing—review, editing, and supervision. M.D.: Conceptualization, methodology, project administration, and funding acquisition. L.L.: Editing and supervision. Y.Z. (Yili Zhang): Editing and supervision. All authors have read and agreed to the published version of the manuscript.

Funding: This research was funded by the second Tibetan Plateau Scientific Expedition and Research Program (Grant No. 2019QZKK0603), the Strategic Priority Research Program of the Chinese Academy of Sciences (XDA20040200), and National Natural Science Foundation of China (Grant No. 42101099).

Data Availability Statement: Not applicable.

Acknowledgments: The authors sincerely thank Zu Jiaxing for his help on the codes and calculation of resistance and resilience.

Conflicts of Interest: The authors declare no conflict of interest.

References

1. Estrada, F.; Kim, D.; Perron, P. Anthropogenic influence in observed regional warming trends and the implied social time of emergence. *Commun. Earth Environ.* **2021**, *2*, 31. [CrossRef]
2. Yu, M.; Li, Q.F.; Hayes, M.J.; Svoboda, M.D.; Heim, R.R. Are droughts becoming more frequent or severe in China based on the Standardized Precipitation Evapotranspiration Index: 1951–2010? *Int. J. Climatol.* **2014**, *34*, 545–558. [CrossRef]
3. Zhao, S.; Cong, D.M.; He, K.X.; Yang, H.; Qin, Z.H. Spatial-Temporal Variation of Drought in China from 1982 to 2010 Based on a modified Temperature Vegetation Drought Index (mTVDI). *Sci. Rep.* **2017**, *7*, 17473. [CrossRef] [PubMed]

4. Vicente-Serrano, S.M.; Gouveia, C.; Camarero, J.J.; Begueria, S.; Trigo, R.; Lopez-Moreno, J.I.; Azorin-Molina, C.; Pasho, E.; Lorenzo-Lacruz, J.; Revuelto, J.; et al. Response of vegetation to drought time-scales across global land biomes. *Proc. Natl. Acad. Sci. USA* **2013**, *110*, 52–57. [CrossRef]
5. Huang, J.; Yu, H.P.; Guan, X.D.; Wang, G.Y.; Guo, R.X. Accelerated dryland expansion under climate Chang. *Nat. Clim. Chang.* **2015**, *6*, 166–171. [CrossRef]
6. Ahlstrom, A.; Raupach, M.R.; Schurgers, G.; Smith, B.; Arneth, A.; Jung, M.; Reichstein, M.; Canadell, J.G.; Friedlingstein, P.; Jain, A.K.; et al. The dominant role of semi-arid ecosystems in the trend and variability of the land CO_2 sink. *Science* **2015**, *348*, 895–899. [CrossRef]
7. Friedlingstein, P.; Meinshausen, M.; Arora, V.K.; Jones, C.D.; Anav, A.; Liddicoat, S.K.; Knutti, R. Uncertainties in CMIP5 Climate Projections due to Carbon Cycle Feedbacks. *J. Clim.* **2014**, *27*, 511–526. [CrossRef]
8. Anderegg, W.R.L.; Schwalm, C.; Biondi, F.; Camarero, J.J.; Koch, G.; Litvak, M.; Ogle, K.; Shaw, J.D.; Shevliakova, E.; Williams, A.P.; et al. Pervasive drought legacies in forest ecosystems and their implications for carbon cycle models. *Science* **2015**, *349*, 528–532. [CrossRef]
9. Wu, D.H.; Zhao, X.; Liang, S.L.; Zhou, T.; Huang, K.C.; Tang, B.J.; Zhao, W.Q. Time-lag effects of global vegetation responses to climate Chang. *Glob. Chang. Biol.* **2015**, *21*, 3520–3531. [CrossRef]
10. Zuo, D.P.; Han, Y.N.; Xu, Z.X.; Li, P.J.; Ban, C.G.; Sun, W.C.; Pang, B.; Peng, D.Z.; Kan, G.Y.; Zhang, R.; et al. Time-lag effects of climatic change and drought on vegetation dynamics in an alpine river basin of the Tibet Plateau, China. *J. Hydrol.* **2021**, *600*, 126532. [CrossRef]
11. Peng, J.; Wu, C.Y.; Zhang, X.Y.; Wang, X.Y.; Gonsamo, A. Satellite detection of cumulative and lagged effects of drought on autumn leaf senescence over the Northern Hemisphere. *Glob. Chang. Biol.* **2019**, *25*, 2174–2188. [CrossRef] [PubMed]
12. Kong, D.X.; Miao, C.Y.; Wu, J.W.; Zheng, H.Y.; Wu, S.H. Time lag of vegetation growth on the Loess Plateau in response to climate factors: Estimation, distribution, and influence. *Sci. Total. Environ.* **2020**, *744*, 140726. [CrossRef] [PubMed]
13. Zhao, A.Z.; Yu, Q.Y.; Feng, L.L.; Zhang, A.B.; Pei, T. Evaluating the cumulative and time-lag effects of drought on grassland vegetation: A case study in the Chinese Loess Plateau. *J. Environ. Manag.* **2020**, *261*, 110214. [CrossRef] [PubMed]
14. Vicente-Serrano, S.M.; Begueria, S.; Lopez-Moreno, J.I. A Multiscalar Drought Index Sensitive to Global Warming: The Standardized Precipitation Evapotranspiration Index. *J. Clim.* **2010**, *23*, 1696–1718. [CrossRef]
15. Vicente-Serrano, S.M.; Camarero, J.J.; Azorin-Molina, C. Diverse responses of forest growth to drought time-scales in the Northern Hemisphere. *Glob. Ecol. Biogeogr.* **2014**, *23*, 1019–1030. [CrossRef]
16. Jiang, P.; Ding, W.G.; Yuan, Y.; Ye, W.F. Diverse response of vegetation growth to multi-time-scale drought under different soil textures in China's pastoral areas. *J. Environ. Manag.* **2020**, *274*, 110992. [CrossRef] [PubMed]
17. Zhang, X.Y.; Zhang, B.Q. The responses of natural vegetation dynamics to drought during the growing season across China. *J. Hydrol.* **2019**, *574*, 706–714. [CrossRef]
18. Jiang, W.X.; Wang, L.C.; Feng, L.; Zhang, M.; Yao, R. Drought characteristics and its impact on changes in surface vegetation from 1981 to 2015 in the Yangtze River Basin, China. *Int. J. Climatol.* **2020**, *40*, 3380–3397. [CrossRef]
19. Ding, Y.X.; Li, Z.; Peng, S.Z. Global analysis of time-lag and -accumulation effects of climate on vegetation growth. *Int. J. Appl. Earth Obs.* **2020**, *92*, 10217. [CrossRef]
20. De Keersmaecker, W.; Lhermitte, S.; Tits, L.; Honnay, O.; Somers, B.; Coppin, P. A model quantifying global vegetation resistance and resilience to short-term climate anomalies and their relationship with vegetation cover. *Glob. Ecol. Biogeogr.* **2015**, *24*, 539–548. [CrossRef]
21. Tilman, D.; Downing, J.A. Biodiversity and stability in grasslands. *Nature* **1994**, *367*, 363–365. [CrossRef]
22. McCann, K.S. The diversity-stability debate. *Nature* **2000**, *405*, 228–233. [CrossRef] [PubMed]
23. Pennekamp, F.; Pontarp, M.; Tabi, A.; Altermatt, F.; Alther, R.; Choffat, Y.; Fronhofer, E.A.; Ganesanandamoorthy, P.; Garnier, A.; Griffiths, J.I.; et al. Biodiversity increases and decreases ecosystem stability. *Nature* **2018**, *563*, 109–112. [CrossRef] [PubMed]
24. Zhang, X.; Fan, Z.F.; Shi, Z.J.; Pan, L.L.; Kwon, S.; Yang, X.H.; Liu, Y.S. Tree characteristics and drought severity modulate the growth resilience of natural Mongolian pine to extreme drought episodes. *Sci. Total. Environ.* **2022**, *830*, 154742. [CrossRef] [PubMed]
25. Li, X.Y.; Piao, S.L.; Wang, K.; Wang, X.H.; Wang, T.; Ciais, P.; Chen, A.P.; Lian, X.; Peng, S.S.; Penuelas, J. Temporal trade-off between gymnosperm resistance and resilience increases forest sensitivity to extreme drought. *Nat. Ecol. Evol.* **2020**, *4*, 1075–1083. [CrossRef] [PubMed]
26. Liu, Y.J.; You, C.H.; Zhang, Y.G.; Chen, S.P.; Zhang, Z.Y.; Li, J.; Wu, Y.F. Resistance and resilience of grasslands to drought detected by SIF in inner Mongolia, China. *Agric. For. Meteorol.* **2021**, *308*, 108567. [CrossRef]
27. Craine, J.M.; Ocheltree, T.W.; Nippert, J.B.; Towne, E.G.; Skibbe, A.M.; Kembel, S.W.; Fargione, J.E. Global diversity of drought tolerance and grassland climate-change resilience. *Nat. Clim. Chang.* **2013**, *3*, 63–67. [CrossRef]
28. Isbell, F.; Craven, D.; Connolly, J.; Loreau, M.; Schmid, B.; Beierkuhnlein, C.; Bezemer, T.M.; Bonin, C.; Bruelheide, H.; De Luca, E.; et al. Biodiversity increases the resistance of ecosystem productivity to climate extremes. *Nature* **2015**, *526*, 574–577. [CrossRef]
29. Gazol, A.; Camarero, J.J.; Vicente-Serrano, S.M.; Sanchez-Salguero, R.; Gutierrez, E.; de Luis, M.; Sanguesa-Barreda, G.; Novak, K.; Rozas, V.; Tiscar, P.A.; et al. Forest resilience to drought varies across biomes. *Glob. Chang. Biol.* **2018**, *24*, 2143–2158. [CrossRef]
30. Gazol, A.; Camarero, J.J.; Anderegg, W.R.L.; Vicente-Serrano, S.M. Impacts of droughts on the growth resilience of Northern Hemisphere forests. *Glob. Ecol. Biogeogr.* **2017**, *26*, 166–176. [CrossRef]

31. Ivits, E.; Horion, S.; Erhard, M.; Fensholt, R. Assessing European ecosystem stability to drought in the vegetation growing season. *Glob. Ecol. Biogeogr.* **2016**, *25*, 1131–1143. [CrossRef]
32. von Keyserlingk, J.; de Hoop, M.; Mayor, A.G.; Dekker, S.C.; Rietkerk, M.; Foerster, S. Resilience of vegetation to drought: Studying the effect of grazing in a Mediterranean rangeland using satellite time series. *Remote Sens. Environ.* **2021**, *255*, 112270. [CrossRef]
33. Huang, K.; Xia, J.Y. High ecosystem stability of evergreen broadleaf forests under severe droughts. *Glob. Chang. Biol.* **2019**, *25*, 3494–3503. [CrossRef] [PubMed]
34. Huang, W.J.; Wang, W.; Cao, M.; Fu, G.; Xia, J.Y.; Wang, Z.X.; Li, J.S. Local climate and biodiversity affect the stability of China's grasslands in response to drought. *Sci. Total. Environ.* **2021**, *768*, 145482. [CrossRef] [PubMed]
35. Che, M.L.; Chen, B.Z.; Innes, J.L.; Wang, G.Y.; Dou, X.M.; Zhou, T.M.; Zhang, H.F.; Yan, J.W.; Xu, G.; Zhao, H.W. Spatial and temporal variations in the end date of the vegetation growing season throughout the Qinghai–Tibetan Plateau from 1982 to 2011. *Agric. For. Meteorol.* **2014**, *189*, 81–90. [CrossRef]
36. Zhang, Q.; Kong, D.D.; Shi, P.J.; Singh, V.P.; Sun, P. Vegetation phenology on the Qinghai-Tibetan Plateau and its response to climate change (1982–2013). *Agric. For. Meteorol.* **2018**, *248*, 408–417. [CrossRef]
37. Piao, S.L.; Cui, M.D.; Chen, A.P.; Wang, X.H.; Ciais, P.; Liu, J.; Tang, Y.H. Altitude and temperature dependence of change in the spring vegetation green-up date from 1982 to 2006 in the Qinghai-Xizang Plateau. *Agric. For. Meteorol.* **2011**, *151*, 1599–1608. [CrossRef]
38. Huang, M.T.; Piao, S.L.; Ciais, P.; Penuelas, J.; Wang, X.H.; Keenan, T.F.; Peng, S.S.; Berry, J.A.; Wang, K.; Mao, J.F.; et al. Air temperature optima of vegetation productivity across global biomes. *Nat. Ecol. Evol.* **2019**, *3*, 772–779. [CrossRef]
39. Zhu, Z.C.; Piao, S.L.; Myneni, R.B.; Huang, M.T.; Zeng, Z.Z.; Canadell, J.G.; Ciais, P.; Sitch, S.; Friedlingstein, P.; Arneth, A.; et al. Greening of the Earth and its drivers. *Nat. Clim. Chang.* **2016**, *6*, 791–797. [CrossRef]
40. Ding, J.Z.; Chen, L.Y.; Ji, C.J.; Hugelius, G.; Li, Y.N.; Liu, L.; Qin, S.Q.; Zhang, B.B.; Yang, G.B.; Li, F. Decadal soil carbon accumulation across Tibetan permafrost regions. *Nat. Geosci.* **2017**, *10*, 420–424. [CrossRef]
41. Liu, L.B.; Wang, Y.; You, N.S.; Liang, Z.; Qin, D.H.; Li, S.C. Changes in aridity and its driving factors in China during 1961–2016. *Int. J. Climatol.* **2019**, *39*, 50–60. [CrossRef]
42. Wang, C.P.; Huang, M.T.; Zhai, P.M. Change in drought conditions and its impacts on vegetation growth over the Tibetan Plateau. *Adv. Clim. Chang. Res.* **2021**, *12*, 333–341. [CrossRef]
43. Wang, Z.Q.; Cui, G.L.; Liu, X.; Zheng, K.; Lu, Z.Y.; Li, H.L.; Wang, G.N.; An, Z.F. Greening of the Qinghai–Tibet Plateau and Its Response to Climate Variations along Elevation Gradients. *Remote Sens.* **2021**, *13*, 3712. [CrossRef]
44. Peng, J.; Jiang, H.; Liu, Q.H.; Green, S.M.; Quine, T.A.; Liu, H.Y.; Qiu, S.J.; Liu, Y.X.; Meersmans, J. Human activity vs. climate change: Distinguishing dominant drivers on LAI dynamics in karst region of southwest China. *Sci. Total. Environ.* **2021**, *769*, 144297. [CrossRef]
45. Zhang, Y.L.; Li, B.Y.; Liu, L.S.; Zheng, D. Redetermine the region and boundaries of Qinghai-Tibet Plateau. *Geogeraphical Res.* **2021**, *40*, 1543–1553. (In Chinese)
46. Ding, J.Z.; Yang, T.; Zhao, Y.T.; Liu, D.; Wang, X.Y.; Yao, Y.T.; Peng, S.S.; Wang, T.; Piao, S.L. Increasingly Important Role of Atmospheric Aridity on Tibetan Alpine Grasslands. *Geophys. Res. Lett.* **2018**, *45*, 2852–2859. [CrossRef]
47. Wang, X.J.; Pang, G.J.; Yang, M.X. Precipitation over the Tibetan Plateau during recent decades: A review based on observations and simulations. *Int. J. Climatol.* **2018**, *3*, 1116–1131. [CrossRef]
48. Chen, J.; Jonsson, P.; Tamura, M.; Gu, Z.H.; Matsushita, B.; Eklundh, L. A simple method for reconstructing a high-quality NDVI time-series data set based on the Savitzky–Golay filter. *Remote Sens. Environ.* **2004**, *91*, 332–344. [CrossRef]
49. Peng, S.Z.; Ding, Y.X.; Wen, Z.M.; Chen, Y.M.; Cao, Y.; Ren, J.Y. Spatiotemporal change and trend analysis of potential evapotranspiration over the Loess Plateau of China during 2011–2100. *Agric. For. Meteorol.* **2017**, *233*, 183–194. [CrossRef]
50. Zheng, D. The system of physico-geographical regions of the Qinghai-Xizang (Tibet) Plateau. Science China. *Earth Sci.* **1996**, *4*, 410–417.
51. Li, M.; Yu, H.L.; Meng, B.P.; Sun, Y.; Zhang, J.G.; Zhang, H.F.; Wu, J.S.; Yi, S.H. Perspectives from the inter-annual variability of vegetation index. *Ecol. Indic.* **2021**, *130*, 108158. [CrossRef]
52. Beguería, S.; Vicente-Serrano, S.M.; Reig, F.; Latorre, B. Standardized precipitation evapotranspiration index (SPEI) revisited: Parameter fitting, evapotranspiration models, tools, datasets and drought monitoring. *Int. J. Climatol.* **2014**, *34*, 3001–3023. [CrossRef]
53. Chen, B.X.; Zhang, X.Z.; Tao, J.; Wu, J.S.; Wang, J.S.; Shi, P.L.; Zhang, Y.J.; Yu, C.Q. The impact of climate change and anthropogenic activities on alpine grassland over the Qinghai-Tibet Plateau. *Agric. For. Meteorol.* **2014**, *189*, 11–18. [CrossRef]
54. Li, M.; Wu, J.S.; Song, C.Q.; He, Y.T.; Niu, B.; Fu, G.; Tarolli, P.; Tietjen, B.; Zhang, X.Z. Temporal Variability of Precipitation and Biomass of Alpine Grasslands on the Northern Tibetan Plateau. *Remote Sens.* **2019**, *11*, 360. [CrossRef]
55. Schwalm, C.R.; Anderegg, W.R.L.; Michalak, A.M.; Fisher, J.B.; Biondi, F.; Koch, G.; Litvak, M.; Ogle, K.; Shaw, J.D.; Wolf, A.; et al. Global patterns of drought recovery. *Nature.* **2017**, *548*, 202–205. [CrossRef]
56. Ma, B.; Zhang, B.; Jia, L.G.; Huang, H. Conditional distribution selection for SPEI-daily and its revealed meteorological drought characteristics in China from 1961 to 2017. *Atmos. Res.* **2020**, *246*, 105108. [CrossRef]
57. Musau, S.; Patil, S.; Sheffield, J.; Marshall, M. Spatio-temporal vegetation dynamics and relationship with climate over East Africa. *Hydrol. Earth Syst. Sci. Dis.* **2016**, 1–30. [CrossRef]

58. Fang, W.; Huang, S.Z.; Guo, Y. Probabilistic assessment of remote sensing-based terrestrial vegetation vulnerability to drought stress of the Loess Plateau in China. *Remote Sens. Environ.* **2019**, *232*, 111290. [CrossRef]
59. D'Orangeville, L.; Maxwell, J.; Kneeshaw, D.; Pederson, N.; Duchesne, L.; Logan, T.; Houle, D.; Arseneault, D.; Beier, C.M.; Bishop, D.A.; et al. Drought timing and local climate determine the sensitivity of eastern temperate forests to drought. *Glo. Chang. Biol.* **2018**, *24*, 2339–2351. [CrossRef]
60. Yin, Y.H.; Ma, D.Y.; Wu, S.H. Enlargement of the semi-arid region in China from 1961 to 2010. *Clim. Dyn.* **2019**, *52*, 509–521. [CrossRef]
61. Wang, J.A.; Zuo, W. *Geographic Atlas of China*; Sinomap Press: Beijing, China, 2010; p. 30.
62. Pardos, M.; del Rio, M.; Pretzsch, H.; Jactel, H.; Bielak, K.; Bravo, F.; Brazaitis, G.; Defossez, E.; Engel, M.; Godvod, K.; et al. The greater resilience of mixed forests to drought mainly depends on their composition: Analysis along a climate gradient across Europe. *For. Ecol. Manag.* **2021**, *481*, 118687. [CrossRef]
63. Choat, B.; Jansen, S.; Brodribb, T.J.; Cochard, H.; Delzon, S.; Bhaskar, R.; Bucci, S.J.; Feild, T.S.; Gleason, S.M.; Hacke, U.G.; et al. Global convergence in the vulnerability of forests to drought. *Nature* **2012**, *491*, 752–755. [CrossRef] [PubMed]
64. Ruppert, J.C.; Harmoney, K.; Henkin, Z.; Snyman, H.A.; Sternberg, M.; Willms, W.; Linstadter, A. Quantifying drylands' drought resistance and recovery: The importance of drought intensity, dominant life history and grazing regime. *Glob. Chang. Biol.* **2015**, *21*, 1258–1270. [CrossRef] [PubMed]
65. Salter, P.J.; Goode, J.E. *Crop Responses to Water at Different Stages of Growth*; Commonwealth Agricultural Bureaux, Farnham Royal: Bucks, UK, 1968; pp. 191–913.
66. Byun, H.R.; Wilhite, D.A. Objective quantification of drought severity and duration. *J. Clim.* **1999**, *12*, 2747–2756. [CrossRef]
67. Vergni, L.; Vinci, A.; Todisco, F. Effectiveness of the new standardized deficit distance index and other meteorological indices in the assessment of agricultural drought impacts in central Italy. *J. Hydrol.* **2021**, *603*, 126986. [CrossRef]
68. Chaves, M.M.; Maroco, J.P.; Pereira, J.S. Understanding plant responses to drought—From genes to the whole plant. *Plant Biol.* **2003**, *30*, 239–264. [CrossRef]
69. Van Ruijven, J.; Berendse, F. Diversity enhances community recovery, but not resistance, after drought. *J. Ecol.* **2010**, *98*, 81–86. [CrossRef]
70. Ye, D.; Gao, Y. *Meteorology of the Qinghai-Xizang (Tibet) Plateau*; Science Press: Beijing, China, 1979; pp. 30–55. (In Chinese)
71. Zeng, P.; Sun, F.Y.; Liu, Y.Y.; Feng, H.Y.; Zhang, R.; Che, Y. Changes of potential evapotranspiration and its sensitivity across China under future climate scenarios. *Atmos. Res.* **2021**, *261*, 105763. [CrossRef]
72. Yao, J.Y.; Liu, H.P.; Huang, J.P.; Gao, Z.M.; Wang, G.Y.; Li, D.; Yu, H.P.; Chen, X.Y. Accelerated dryland expansion regulates future variability in dryland gross primary production. *Nat. Commun.* **2020**, *11*, 1665. [CrossRef]
73. Huang, J.; Li, Y.; Fu, C.; Chen, F.; Fu, Q.; Dai, A.; Shinoda, M.; Ma, Z.; Guo, W.; Li, Z.; et al. Dryland Climate Change: Recent Progress and Challenges. *Rev. Geophys.* **2017**, *55*, 719–778. [CrossRef]
74. Ji, M.X.; Huang, J.P.; Xie, Y.K.; Liu, J. Comparison of Dryland Climate Change in Observations and CMIP5 Simulations. *Adv. Atmos. Sci.* **2015**, *32*, 1565–1574. [CrossRef]
75. Zhang, H.M.; Ding, M.J.; Li, L.H.; Liu, L.S. Continuous Wetting on the Tibetan Plateau during 1970–2017. *Water* **2019**, *11*, 2605. [CrossRef]
76. Zhang, H.Y.; Fan, J.W.; Cao, W.; Zhong, H.P.; Harris, W.; Gong, G.L.; Zhang, Y.X. Changes in multiple ecosystem services between 2000 and 2013 and their driving factors in the Grazing Withdrawal Program, China. *Ecol. Eng.* **2018**, *116*, 67–79. [CrossRef]

Disclaimer/Publisher's Note: The statements, opinions and data contained in all publications are solely those of the individual author(s) and contributor(s) and not of MDPI and/or the editor(s). MDPI and/or the editor(s) disclaim responsibility for any injury to people or property resulting from any ideas, methods, instructions or products referred to in the content.